



Experimental and Numerical Investigation of Octagonal Partially Encased Composite Columns Subject to Axial and Torsion Moment Loading

Mehdi Ebadi Jamkhaneh ^{a*}, Mohammad Ali Kafi ^b

^a Ph.D. Candidate, Civil Engineering Faculty, Semnan University, Semnan, Iran.

^b Associate Professor, Civil Engineering Faculty, Semnan University, Semnan, Iran.

Received 13 September 2017; Accepted 23 October 2017

Abstract

This paper includes experimental and numerical study of the octagonal partially encased composite (PEC) columns specimens under axial and torsion loading. The major difference between them was the concrete reinforcement details. The parameters investigated in the experimental and numerical study were the type of reinforcement details, the failure mode, width-to-thickness ratio of flange, transverse links spacing and diameter. The results were presented as load-deformation curves. Numerical model was validated using finite element method and the results indicated acceptable accuracy with tests results in the form of capacity and ductility. In the analytical phase, the experimental results in the compressive loading were compared with those obtained from CSA S16-14 and EN 1994-1-1 equations. Also, the new concrete confinement factor in proportion to the web width to thickness ratio was presented to octagonal PEC columns under pure compressive load. Furthermore, different types of retrofit of cross-shaped steel column including concrete encasement, use of stiffener plates and transverse links were investigated in this research. Results revealed that concrete confinement and use of transverse links had respectively the most and the least effect on increasing torsional capacity of the specimens.

Keywords: Octagonal Partially Encased Composite Column; Failure Mode; Experimental Model; Finite Element Method; Load Bearing Capacity; Torsional Stiffness.

1. Introduction

Steel-concrete structures improve the seismic performance of structures and stiffness of high-rise buildings [1, 2]. Taking benefit from composite sections is of high importance in construction and tall buildings industry [3]. On the other hand, using of two material properties lead to increase the energy absorption [4]. The Partially Encased Composite (PEC) column is one of the recent achievements in the field of composite columns. Usually, PEC columns are made out of three plates filling the gap between the flange and web is filled using concrete. In the common samples in European countries and Canada, web and flange thicknesses are considered as equal. Meanwhile, in order to prevent flanges local buckling strength from increasing, transverse links are welded to the flange tip between the flanges on equal intervals. In Europe, hot-rolled compressed standard sections are used which are inherently resistant against local buckling. The concrete casted between the flanges both provide a certain part of the column axial compressing strength and prevent column web from local buckling. Moreover, flanges deformation towards the column internal part is prevented. On the

* Corresponding author: mehdi.ebadi@semnan.ac.ir

 <http://dx.doi.org/10.28991/cej-030927>

➤ This is an open access article under the CC-BY license (<https://creativecommons.org/licenses/by/4.0/>).

© Authors retain all copyrights.

other hand, transverse links prevent the flanges deformation outwardly. Therefore, using of these types of composite column has a wide benefit that recently, researchers have paid attention to this.

Regarding the PEC columns, several scholars have studied their behaviour under axial, bending and shear loading in experimental and numerical methods. Chicoine et al. [5] suggested a numerical model to study the concrete confinement effect, remained stresses and imperfections in the flanges on total column behaviour. Furthermore, in another study [6], they assessed the parameters effective on the behaviour of such columns, link spacing, flange stiffness, longitudinal and transverse reinforcements. Begum et al. [7] modelled finite element of PEC columns under different loading conditions using dynamic explicit solution strategy. PEC columns with thin-walled filled with high strength concrete behaviour were studied by Begum et al. [8]. The results indicated brittle failure of these columns in comparison to utilization of concrete with normal strength. Begum et al. [9] conducted parametric study on eccentrically-loaded PEC columns under major axis bending. Chen et al. [10] conducted a series of experimental and numerical tests on PEC columns under axial and cyclic loading. They concluded the transverse links spacing is effective to prevent column flange local buckling with high width to thickness ratio. Zhao and Feng [11] investigated axial ultimate capacity of PEC columns. Their results show a closer link spacing improves the ductility of the columns; however, the measurements show that in general yielding do not occur before the peak load in the links. In an experimental research, researchers [12] used the PEC columns in a steel shear wall system. The test results indicated detailing of the PEC columns played an important role in improving the seismic performance of the system. Pereira et al. [13] studied PEC columns behaviour under pure axial loading under the presence of longitudinal and transverse steel bars. They demonstrated effects of bar presence on load bearing capacity, stiffness and post-peak behaviour are not really significant. Song et al. [14] investigated local and post-local buckling behaviour of welded steel shapes in PEC columns. Based on their parametric study, a series of expressions was developed for predicting critical strength and post-buckling strength in PEC columns under concentric loading. Ebadi Jamkhaneh et al. [15] studied three types of octagonal PEC columns under axial loading as experimental and numerical models.

In all previous works, researchers used PEC columns fabricated with hot-rolled H-shaped cross-section or sections with the same thickness of flange and web. In spite of all above mentioned studies, there is a lack of comprehensive investigation on the influence of different thickness of thin-walled, shape of steel section, and length of welding line. In this study, different thickness for flanges and webs is used for cross-shaped steel profile (flange thickness is twice of web thickness) due to the same inertial moments in both directions, symmetry of section, easy implementation, and possible connection in any direction. It should be noted that the proposed column is examined under axial, eccentrically compressive and torsion load. One of the main disadvantages of cross-shaped steel section is its low torsional resistance. To improve the torsional resistance of this type of sections, transverse links are spaced between the flange tips and filled by concrete. To the best of the authors' knowledge, there are no researches on the torsional behaviour of PEC columns. Generally, in this research, the key objectives of the experimental and numerical parametric study are acquiring better understanding of the effect of key parameters (slenderness ratio of flange, material property, interval spacing of links, and welding line configurations) on the behaviour of PEC column, capturing the effects of concrete, transverse links, and length of welding line on the axial and eccentrically compressive strength, and proposing a new practical equation for PEC column. Finally, torsional behaviour of these members assessed with variety of parameters. Details of the studies have been explained in the following sections of this paper.

2. Research Methodology

After an extensive literature review on the PEC columns, studying the behaviour of these columns was conducted using experimental and numerical methods. Laboratory and numerical studies were presented. First, three small scale test specimens were presented and the results were discussed. In the next phase, several numerical models were presented for parametrical studies. In the numerical section, the test model verification and parametric studies were presented. Finally, according to the numerical studies, a relationship was presented to calculate the compressive load-bearing capacity of the PEC columns.

2.1. Experimental Investigation

Three one-third-scale PEC columns measuring (width×depth×height) $150 \times 150 \times 1000 \text{ mm}$ were constructed. Figure 1. shows typical PEC column geometric parameters. Parameters illustrated in the concrete-side elevation view (Figure 1a) are the column length, L , and the centre-to-centre spacing of the links, s . Parameters illustrated in the plan view (Figure 1b) are the column depth, d , the overall flange width, b_f , the flange thickness, t_f , and the web thickness, t_w . The steel section was fabricated from st37 grade. The nominal plate thickness of flange and web were 6 mm and 3 mm , respectively. The nominal flange width-to-thickness ratio for the columns was 10. This value was lower than the maximum flange width-to-thickness ratio of 32 specified by CSA S16-14 [16]. The columns had a constant link spacing equal to 100 mm and all of the links had a diameter of 6 mm . Transverse links were welded in flange internal space with a rough distance of 10 mm from the flange tip to the inside thereof. Eventually, a rough 10 mm concrete coverage was placed on the links without considering the link diameter. Eight columns were cast with normal-strength (nominally 25

MPa) concrete in the test region. A summary of the PEC columns characteristics is listed in Table 1. The column ending areas (50 mm above and beneath the column) were strengthened to prevent premature yielding caused by applicable load.

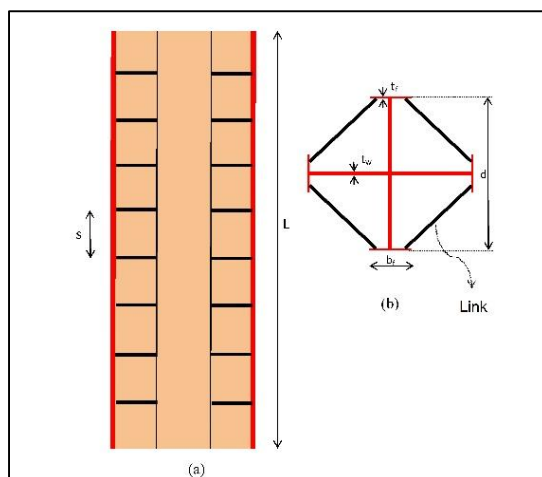


Figure 1. Geometry of PEC column in (a) steel-side elevation, and (b) plan view

2.1.1. Material Properties

The main properties of interest during the mix design were strength and workability. Their mix designs are presented in Table 2. The concrete was made with locally available materials. 0.0125 m crush coarse aggregate was used. The fine aggregate had a fineness module of 2.4. Considering that the typical concrete density of the mixes was 2300 kg/m³, the elastic modulus of the normal-strength concrete (23.715 GPa) was within typical ranges of American Concrete Institute’s (ACI) Manual of Concrete Practice report ACI-318-08 [17], Section 8.5.1. The average strain at peak stress of the normal-strength concrete was 2225 με, which was a typical value. The Poisson’s ratio of the normal-strength concrete (0.13) was typical of accepted values (0.11 to 0.21) for normal-strength concrete according to the ACI report 363R-92 [18].

Table 1. Characteristics of test specimens

Column	PEC-C	PEC-CL	PEC-CLS
$b \times d$ (mm)	60 × 150	60 × 150	60 × 150
Length, L (mm)	1000	1000	1000
Thickness of flange, web (mm)	6,3	6,3	6,3
Flange width to-thickness ratio, (b_f/t_f)	10	10	10
Link	Spacing (mm)	100	100
	Diameter (mm)	6	6
Longitudinal bar	Number	0	4
	Diameter (mm)	0	14
Stirrup	Spacing (mm)	0	100
	Diameter (mm)	0	6

Table 2. Concrete mix design

Material	Water	Cement	Coarse aggregate	Fine aggregate	W/C
Weight (kg)	215	430	1053.15	616.85	0.5

All coupon tests were conducted in an MTS 1000 universal testing machine, with a tensile capacity of 1000 kN, at the Structural Engineering Laboratory of Semnan University. Load measurements were taken using the internal load cell of the MTS 1000. The stress versus-strain curves generated were typical of hot-rolled structural grade steels. All links of a particular diameter were cut from rods of the same heat of steel, as were additional pieces acquired for material testing. Four tension coupons were tested from the steel rods. Two of the coupons were cut from the 6 mm steel rod used as links. The other two were cut from the 14 mm steel rod used as longitudinal rebar. The coupons were tested

according to ASTM Standard A370 [19] shown in Table 3. Also, welding was performed using E60xx electrodes, and the ultimate tension and strain of fillet welds were taken as 420 MPa and 0.6%.

Table 3. Tensile test results for steel plate and steel rod

	Static Yield Stress (MPa)	Static Ultimate Stress (MPa)	Elastic Modulus (MPa)	Yield Strain (μϵ)	Hardening Strain (μϵ)	Rupture Strain (μϵ)
Steel Plate	257	389	202100	1951	16900	320000
Steel Rod	297	412	195600	1568	23200	451000

2.1.2. Test Setup and Procedures

All PEC columns were tested at the structural laboratory in Semnan University. Three of the columns (PEC-C through PEC-CLS) were tested with fixed-end condition in one side and vertical slide in another side. Test of the columns under concentric compressive loading was performed using a testing system machine that had a loading capacity of 2 MN. The loadcell applied a compressive force horizontally, and hydraulic jack had a maximum stroke of 400 mm. The base of the universal testing system (UTS) sat horizontally on a frame. The loading procedure was similar for each of the three tests. Primary force rate (5 kN/min) was used to control the UTS. The test began at a force rate of 50 kN/min until the displacement reached approximately 0.05 mm, during which the electronic data were scrutinized to ensure that all channels were functioning properly. Following this, the force rate was increased to 75 kN/min until the real-time graphs of the column behaviour indicated that the column stiffness was decreasing (typically about 80% of the peak load). To minimize dynamic effects, the force rate was then decreased back to 50 kN/min until failure of the column occurred. If the failure resulted in a sudden drop in column capacity, the force of the UTS was held constant until the measured UTS displacement had stabilized and photographs had been taken. Loading was then changed to displacement control at a stroke rate of 0.06 mm/min. If the failure resulted in a gradual drop in capacity, the stroke rate was held at 0.06 mm/min until the column capacity was reduced to below 85% of the peak load. Then, the rate was increased to 0.08 mm/min. Regardless of the failure type, once the degradation of post-peak strength began to slow significantly, defining a reasonably stable residual strength plateau, the stroke rate was increased to 0.1 mm/min. The column was then unloaded and the unloading behaviour was recorded. Figure 2. shows the concentric load test setup.

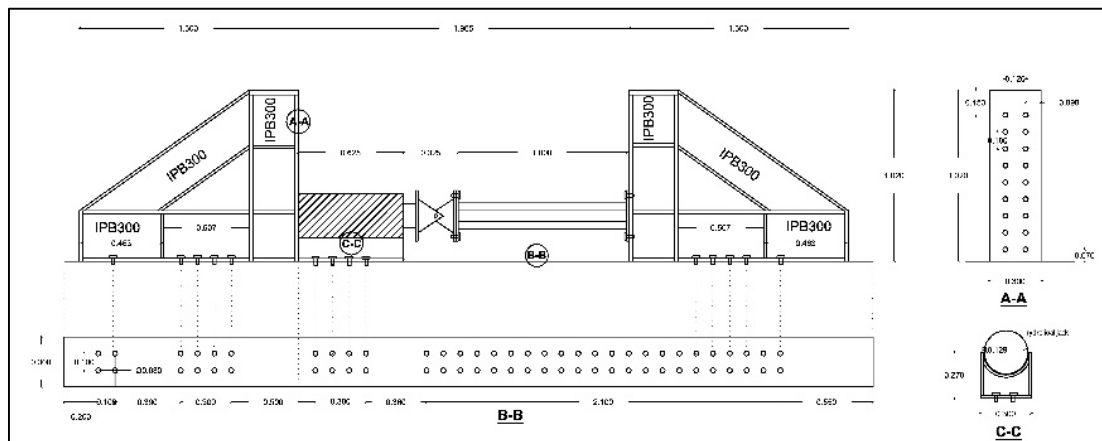


Figure 2. Setup for concentric compression loading (Units: mm)

2.1.3. Experimental Results and Discussion

2.1.3.1. Comparison between Analytical Eq. and Experimental Results

A summary of the peak test loads and predicted loads in codes (CSA S16-14 [16] and EN 1994-1-1 [20]) for the three PEC columns that were loaded concentrically is presented in Table 4. The predicted column load was computed using Equations 1 and 2.

$$C_{rc} = (\phi A_{se} F_y + 0.95 \alpha_1 \phi_c A_c f'_c + \phi_r A_r F_{yr}) (1 + \lambda^{2n})^{1/n} \tag{CSA S16-14 (1)}$$

$$N_{pl,Rd} = A_s f_{yd} + A_s f_{sd} + 0.85 A_s f_{cd} \tag{EN1994 (2)}$$

$N_{pl,Rd} = C_{rc}$ = The factored compressive resistance, $\phi = 0.90$ (Resistance factor of structural steel), $\phi_c = 0.65$ (Resistance factor of concrete), $\phi_r = 0.85$ (Resistance factor of reinforcing steel bars), A_{se} = Effective steel

area of the steel section, A_c = Area of concrete, A_r = Area of longitudinal reinforcement, $f_{sd}= F_y$ = Yield strength of steel plate, $f_{cd} = f'_c$ = Compressive strength of concrete, $f_{yd} = F_{yr}$ = Yield strength of steel bar, λ = Slenderness parameter, $\alpha = 0.85 - 0.0015f'_c$ (but not less than 0.73), and $n = 1.34$.

$$\lambda = \sqrt{\frac{C_p}{C_{ec}}} \tag{3}$$

$$C_{ec} = \frac{\pi^2 EI_e}{(KL)^2} \tag{4}$$

$$EI_e = EI_s + \frac{0.6E_c I_c}{1 + \frac{C_{fs}}{C_f}} \tag{5}$$

C_{fs} = Sustained axial load on the column, C_f = Total axial load on the column, I_s and I_c = moment of inertia of the steel and concrete areas, respectively, as computed with respect to the centre of gravity of the cross-section, $C_p = C_{rc}$ computed with ϕ, ϕ_c and $\phi_r = 1.0$ and $\gamma = 0$, C_{ec} = Critical loading, E_c = Modulus of elasticity of concrete, E = Modulus of elasticity of steel, KL = Effective length of column, and I_e = Equivalent moment of inertia.

Since the test specimens were stub columns, their slenderness parameter, λ , was set to zero for the calculation of the column capacity. For all three test specimens, the test load exceeded the predicted capacity from CSA S16-14 equation. The columns containing steel rebar, PEC-CL and PEC-CLS, had the highest test-to-predicted load corresponding to the CSA S16-14 equation ratios, 1.23 and 1.32, respectively. CSA S16-14 design calculations reduced the capacity of the steel flanges to account for their susceptibility to local buckling between the links.

Table 4. Comparison of peak test loads between experimental and predicted results

Specimen	$P_{(Exp)}$ (kN)	$P_{(CSA\ S16-14)}$ (kN)	$P_{(EN\ 1994-1-1)}$ (kN)	$P_{(Exp)}/P_{(CSA\ S16-14)}$	$P_{(Exp)}/P_{(EN\ 1994)}$
PEC-C	802.53	688.285	875.881	1.166	0.916
PEC-CL	1105	895.605	1117.033	1.234	0.989
PEC-CLS	1180	895.605	1117.033	1.317	1.056

2.1.3.2. Load-Displacement Curves

Figure 3. shows the axial load-displacement responses of the three concentric tested specimens. The values of initial stiffness, maximum load, and displacement are presented for each specimen in Table 5. PEC-CLS specimen had the maximum compressive and elastic stiffness capacity in comparison to the two other specimens. PEC-CLS specimen compressive capacity was 1.47 and 1.07 times higher than PEC-C and PEC-CL, respectively. Also this specimen stiffness was 24% bigger than that of PEC-C.

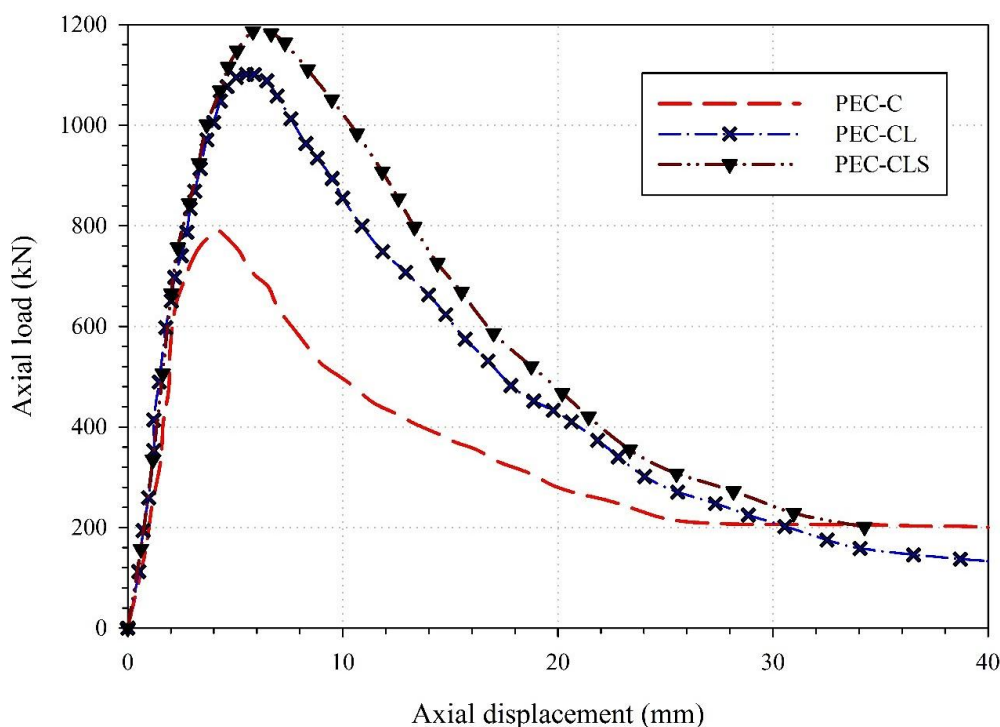


Figure 3. Axial load-displacement curves of specimens

Higher stiffness of PEC-CLS column in comparison with other columns was the result of using L-shaped stirrups covering the longitudinal rebars which led to more confinement and thus increased the column strength. Additionally, it was observed that presence of concrete in PEC specimens reduced the lateral deflections by 70%.

Table 5. Results of specimens under compressive loading

Specimen	P (kN)	Δ (mm)	K (kN/mm)
PEC-C	802.53	4.02	216.62
PEC-CL	1105.00	5.37	234.15
PEC-CLS	1180.00	8.66	269.51

2.1.3.3. Failure Mode

All columns had a similar failure mode- concrete crushed content plus local buckling of flanges- except for column PEC-C which had a link weld fracture followed by concrete crushing combined with local buckling of the flanges. No local buckling of the flanges was observed for any of the columns before the peak load was reached. Although the failure modes were similar for all columns, the point at which the failure (marked by a sudden drop in load-bearing capacity) occurred, as compared to the peak capacity, was different depending on the presence or absence of steel rebar and stirrups. Columns exhibited sudden failure at their peak load. Typically, the failure region was located between adjacent links (Figure 4a). Distinct shear-failure planes were exposed by removing the crushed concrete after the test. The depths of the shear planes were related to the link spacing. For the closest link spacing the shear-failure plane was only as deep as the links themselves. This resulted in small amounts of concrete spalling off of the column. However, for the largest link spacing or fracture of links (200 mm), the shear-failure plane extended to a point closer to the web than the concrete surface. This resulted in large pieces of concrete exploding out of the column as failure took place. The relationship between the shear-plane depth and the link spacing was expected since the closer link spacing provided a higher degree of confinement to the concrete.

Before reaching the peak loading in specimen PEC-C, minor cracking at the end of column and removing the priming paint on flange faces occurred. A sudden drop in capacity occurred immediately after reaching the peak load (802.53 kN). At the peak load, side flanges buckled and the concrete adjacent to the left side of column was crushed (Figure 4a). Two bangs were heard as the link welds fractured when the load reached to 600 kN. Throughout the post-peak loading, web plates were buckled at 200 mm top of column. Immediately thereafter, upper flange situated near the end support, buckled at 480 kN. Near the end of the test, the weld between the second link in the first 200 mm and the flanges fractured. By fracturing of the welds, the unsupported flange length increased which resulted in ultimate buckling of the flange; the lengths of this fractured zone was approximately 300 mm which extended into adjacent zones

gradually. During the failure of specimen PEC-CL, cracks were evident in the first 200 mm and light spalling of the concrete took place on this zone (Figure 4b). After sudden drop in capacity, the concrete near the support was crushed and the upper and bottom flanges buckled. During the post-peak loading, a transverse crack propagated along the centreline of the links. The fillet weld between the flange and web plate fractured through the post-peak period.

Additionally, at the peak load, buckling of longitudinal rebars occurred which resulted in cracking and spalling of the concrete. In specimen PEC-CLS, before capacity load reached the peak load, light spalling of the concrete took place at 800 kN which started to propagate longitudinally at 950 kN. Immediately, after the peak load, the concrete cover crushed in mid-span and at the base and a large piece of concrete spalled from the column, landing near the column base (Figure 4c). As this occurred, the flanges at the base underwent local buckling. At the same time, the fillet welds of the links fractured at 140 kN during testing.



Figure 4. Buckling of flanges and crushing of concrete in specimens: (a) PEC-C, (b) PEC-CL, (c) PEC-CLS

2.1.3.4. Comparison of Column Behaviour to Constituent Behaviour

The strength of PEC columns is a summation of the strength of the steel and concrete section (see Equations 1 and 2). Observations made during testing and information obtained from the analysis of the measurements indicated that in general buckling did not occur before the peak load. The behaviour of the steel and the concrete components could be superimposed as a means to study the overall column behaviour. Figure 5 illustrates the superimposed constituent strengths compared with the actual column behaviour for columns PEC-C through PEC-CLS. The concrete strength was calculated by multiplying the concrete area, A_c , by the corresponding measured concrete stress, f_c , from the average cylinder test curve for that mix. Similarly, the steel plate and rebar strength was calculated by multiplying A_s and A_r by the steel stress, F_s and F_r , measured from the tension coupons. At the peak load for each column, F_s equals F_y and f_c equals f'_c . Two combinations of superimposed constituent strengths are illustrated to be compared with the actual column behaviour. According to Equation 2, the steel and concrete strength plots are combined. The summation of the material behaviour provided a simple model to be compared with the actual column behaviour.

For column PEC-C, the measured column load was lower than that predicted by $A_s F_s + 0.8 A_c f_c$ for the majority of the pre-peak behaviour and was close to this value at low column loads. Therefore, the column utilized the full steel section. The column reached its peak load at a higher strain than what predicted by constituent summation (see Figure 5a). The resulted high strain values were due to the concrete confinement by the links. Therefore, presence of links improved the failure mode of PEC columns. After the peak column load, the constituent summation predictions dropped rapidly as the concrete material model did not benefit from any confinement. Due to utilization of four longitudinal rebars in column PEC-CL and presence of stirrups in column PEC-CLS, a 15% increase of strain at peak load was

observed in these columns (Figure 5b and 5c). Both specimens' linear behaviours were consistent with summation formula of $A_{rFr} + A_{sFs} + 0.8A_{cfc}$. Post-peak behaviour could not be compared because the constituent summation predictions did not reach the column strain at the peak load.

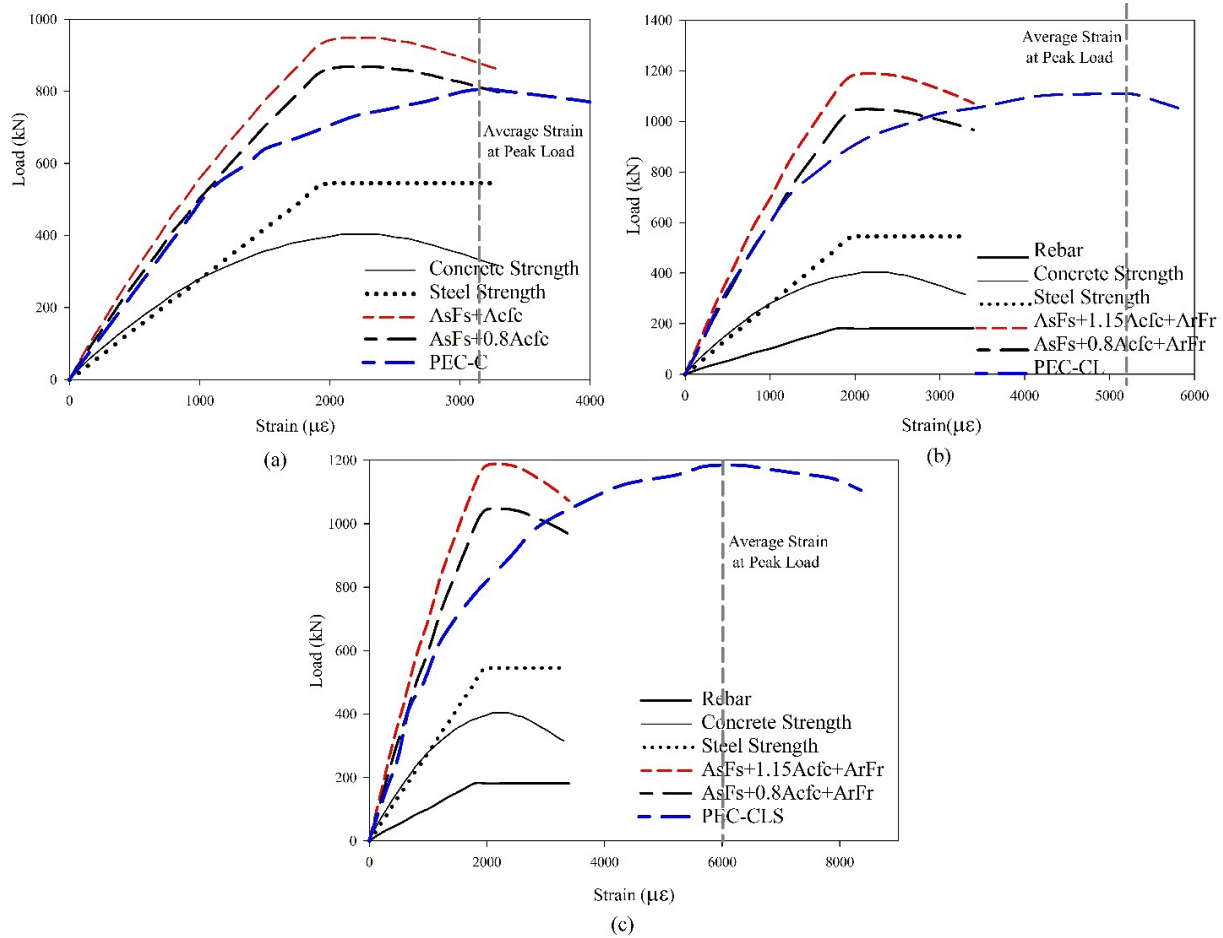


Figure 5. Analytical strength of PEC specimens: (a) PEC-C, (b) PEC-CL, and (c) PEC-CLS

2.2. Numerical Simulation

The tested specimens were simulated using ABAQUS v6.13.1 [22] software. All of the details of specimens, interactions, boundary conditions, and materials were accurately modelled based on the test reports. The columns steel sections were composed of thin plates which were exposed to buckling. In numerical model, due to big deformations along such thin section, nonlinear geometry was added to the relevant behaviour. In the tested specimens, when PEC-C reached the peak capacity, concrete crushed and local buckling of flange steel section occurred simultaneously. In order to consider such type of behaviour, S4R element for steel plate and C3D8R element were used for concrete and welds modelling. The transverse links and longitudinal rebars were modelled using B31 beam elements, which was a special beam element using linear interpolation and allowing for transverse shear deformation. The interactions between the concrete and the steel section, including steel flanges and web, were simulated in the model, since there was no separation between the concrete and steel section until local buckling occurred in the column flanges. The contact pair algorithm was chosen to model the interactions in the columns. The penalty contact algorithm was finally chosen. The basic Coulomb friction model was used in the penalty contact algorithm, in which the tangential forces in the contacted surfaces were modelled. The concrete plasticity damages model was used in ABAQUS finite element program to simulate the concrete behaviour under monotonic load. Here, it was presumed that the tensile cracking and compressive crushing were two major yield mechanism of concrete substance. The tensile and compressive damage parameters changed linearly in proportion to the inelastic strain.

A mesh density sensitivity analysis was performed with the S4R and C3D8R elements to optimise the mesh in order to produce proper representations of local buckling of the steel flange and simultaneous concrete crushing, while maintaining reasonable computing economies. For all the elements except the elements defined at the web-flange junction, the aspect ratio was close to 1.0. At the corner where the plates meet, narrow elements with a width equal to one-half the thickness of the plates were defined to match the mesh of the steel plates with that of the concrete. Maximum and minimum sizes of steel plate were 2 mm and 0.5 mm, respectively. All continuum and plate elements in ABAQUS

[22] were based on an updated Lagrangian formulation. This formulation was useful for the current problem because the elements experienced considerable shape changes resulting from large rotations due to local buckling of the flange plates. To account for the shape change, the nodal coordinates were updated at the beginning of each increment to reflect current positions in space, and all the shape functions and derivatives were re-evaluated using the updated nodal coordinates.

The boundary conditions applied in the model to simulate the end conditions for both the concentrically and torsional loaded specimens were presented. These constraints were applied through a reference node situated in each of the top and bottom rigid surfaces of the finite element model. For the concentrically loaded columns, translations and rotations at both ends were fixed, except for the vertical displacement at the top. In the finite element model for torsional loaded test specimens, pinned-pinned end conditions were applied at the eccentric load points located on the top rigid end planes. Bottom of column was fixed.

The model introduced by Hsu and Hsu [23] was used to define concrete stress-strain behavioural model in the compressive area. This behavioural model has been presented for the concrete with compressive strength up to 62 MPa. This model calculates compressive stress values from $0.5\sigma_{cu}$ on the ascending part to $0.5\sigma_{cu}$ on the descending part. In this model, compressive stress was found through Equations 8 to 10.

$$\sigma_c = \left(\frac{\beta \left(\frac{\epsilon_c}{\epsilon_0} \right)}{\beta - 1 + \left(\frac{\epsilon_c}{\epsilon_0} \right)^\beta} \right) \sigma_{cu} \tag{8}$$

$$\beta = \frac{1}{1 - \left[\frac{\sigma_{cu}}{\epsilon_0 E_0} \right]}, \quad \epsilon_0 = 8.9 \times 10^{-5} \sigma_{cu} + 2.114 \times 10^{-3} \tag{9}$$

$$E_0 = 1.2431 \times 10^2 \sigma_{cu} + 3.28312 \times 10^3 \tag{10}$$

In this study, Nayal and Rashid’s model [24] was used to plot the stress-strain relationship at the tension area. In order to prevent runtime error, there was a decrease from ultimate stress σ_t to $8\sigma_t$ in ABAQUS software. Equation 11 was used to find maximum tensile stress.

$$\sigma_t = 0.3(\sigma_c)^{\frac{2}{3}} \tag{11}$$

The nonlinear behaviour of steel and weld elements were simulated using an isotropic hardening model based on the Mises yield criterion. The model replicated the experimental PEC-C and numerical simulation as shown in Figure 6.

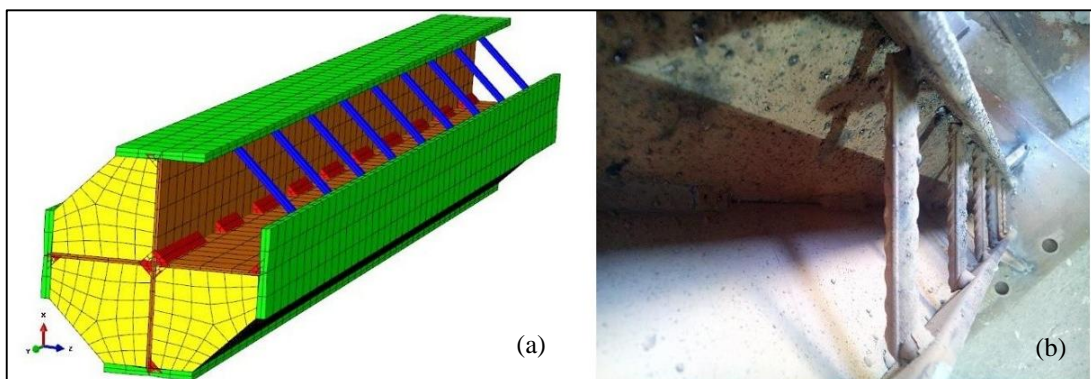


Figure 6. (a) The numerical validation model using ABAQUS and (b) experimental PEC-C test

2.2.1. Comparison of Numerical Simulation with Test Results

In this section, to assess the capability of the developed numerical model in simulating the PEC columns, the results of the conducted tests are employed to verify and calibrate the developed numerical model in ABAQUS. In simulation of loading condition, a given displacement control in test PEC-C was imposed. Figure 7. show the comparison of finite element method with the test results. Comparing the charts in two linear and non-linear areas showed a good agreement

in the initial elastic stiffness and slope of the second part of the graph. It can be understood that the numerical model and material constitutive adopted in this paper are reasonable. Figure 8 indicates the buckling faces and concrete crushing at the peak load in numerical model and experimental test of PEC-C. Analyses were executed to validate the performance to local buckling under compressive stress of shell elements used for the steel and the axial capacity of concrete brick elements used for the concrete. Various parameters such as slenderness ratio of the flange, welding line length, transverse links diameters and the interval distance between links in numerical models and their effect on the suggested PEC behaviour were considered. Upon conducting parametric studies and analysis using finite element method, the effect of foregoing parameters on PECs load-bearing capacity and formability were studied. Four of most important factors, the interval distance and diameter of links, length of welding line, and the width-thickness ratio of steel plates are demonstrated.

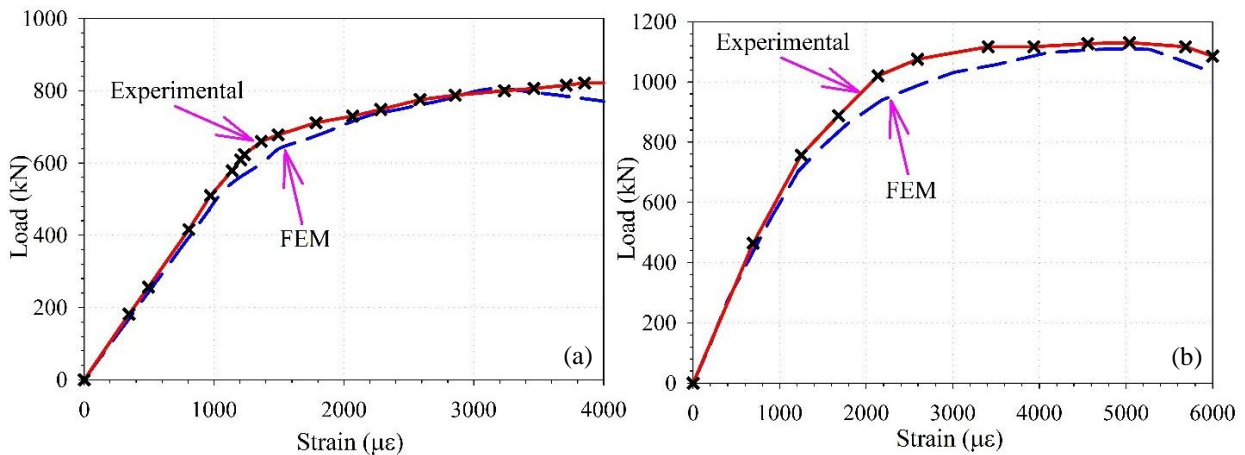


Figure 7. Comparison of load-displacement curve between FEM and experimental results of column (a) PEC-C and (b) PEC-CL

2.3. Parametric Study

2.3.1. Link Spacing

The distance between links defined as a free distance significantly affected the columns behaviour. The local buckling of the suggested section resulted in a decrease in capacity and formability of such type of columns. According to the results, the reduction of load-bearing capacity for the specimens with the links interval distance with 50 mm has a more gradual trend in comparison to 100 mm intervals. In Figure 9, such trend has been indicated in force-displacement curve for PEC-CL column with a variety of links intervals. The closer interval had better loading capacity and deformability. The long interval space between the links due to the link broken weld resulted in formation of deep shearing cracks and decreased loading bearing capacity. The broken welds or links in turn caused a decrease in concrete confinement effect which automatically reduced column load bearing capacity as well. This issue was observed in using 200 mm intervals among the links in comparison to the shorter intervals.

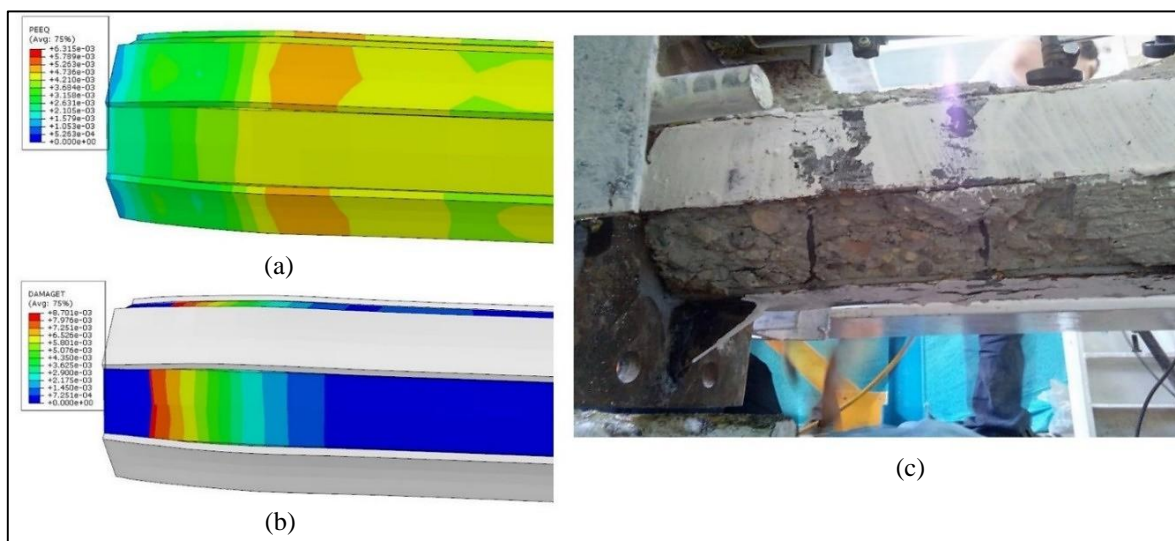


Figure 8. Buckling faces and concrete crushing at the peak load of column PEC-C

2.3.2. Diameter of Transverse Links

Figure 10. shows the effect of different diameter on the behaviour of columns. Lack of transverse link has resulted in early loss in column load-bearing capacity, which emanated from early buckling of the relevant steel beam flanges. However, no significant changes were observed in column load-bearing capacity. Therefore, it may be expressed that the effect of link presence/non-presence is far more significant than that of transverse link diameter.

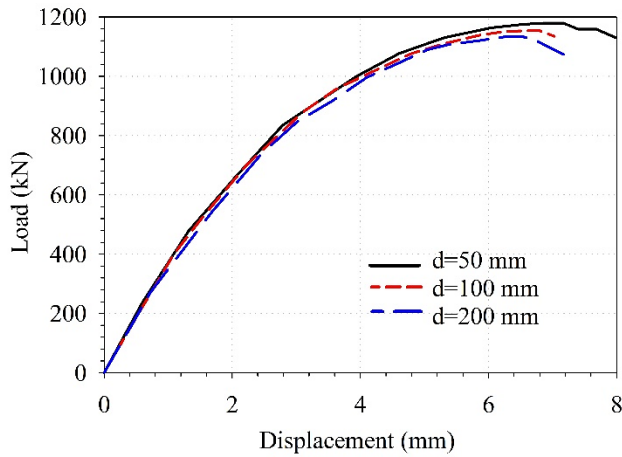


Figure 9. Comparison of transverse link intervals in specimen PEC-CL

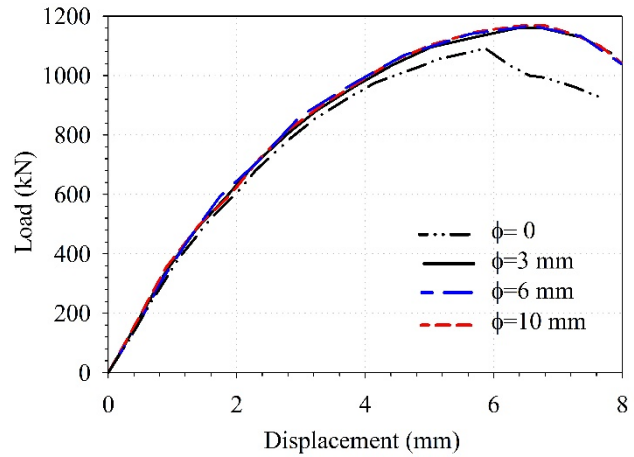


Figure 10. Comparison of influence of diameter transverse links of specimen PEC-CL

2.3.3. Width-Thickness (Slenderness) Ratio of Flange

This section describes the limiting slenderness ratios compression flanges. The slenderness ratio for flanges is denoted as Ratio, and is equal to 5, 10, 20, and 30 for column PEC-CL. These values were lower than the maximum flange width-to-thickness ratio of 32 specified by CSA S16-14. Figure 11. depicts the behaviour of column PEC-CL with different Ratio. According to numerical results of non-linear static analyses, columns with bigger flange width-to-thickness ratios experienced less strength in comparison to column with bigger flange thickness. Meanwhile, sudden strength loss was seen in columns with bigger width-to-thickness ratios after load peak. Such big flange width-to-thickness ratio resulted in commencement of early non-linear behaviour in comparison to smaller ratio state. The load-bearing capacity was decreased roughly 52% by increasing the flange width-to-thickness ratio from 5 to 30. On the other hand, it was observed that by decreasing such ratio the maximum load resulted deflection was also decreased accordingly, which was due to flange premature buckling.

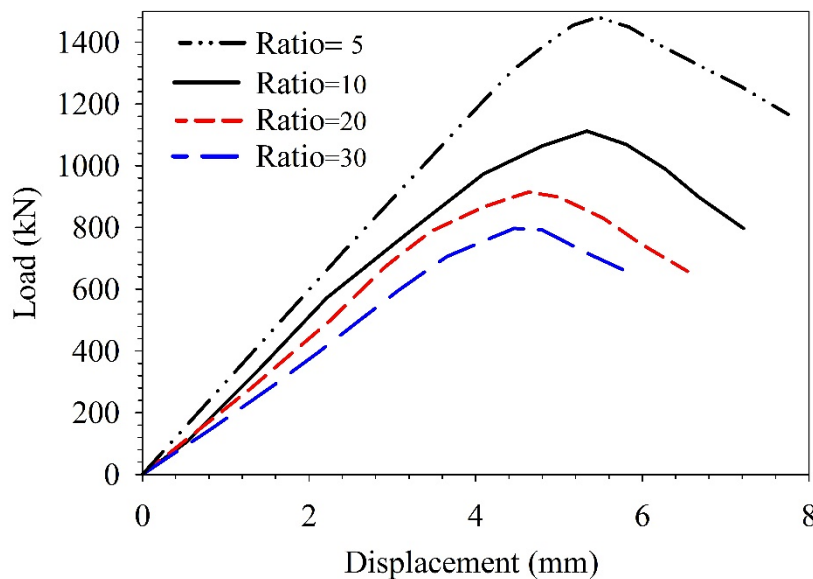


Figure 11. Comparison of width-thickness ratio of flange of specimen PEC-CL

2.4. Practical Formula for Load Bearing Capacity

The stress and tensile damage contour at the ultimate state for specimen PEC-C is extracted from the FE model and shown in Figure 12a to 12c. According to the above figure, the stress distribution of the octagonal PEC columns can be summarized as Figure 12d. This issue is due to the fact of stress distribution and the superposition principle, where A_{c1} is the unconstrained area of concrete, A_{c2} is the constrained area of concrete, and A_c is the cross-sectional area of concrete. In this way, the following relations can be expressed:

$$A_c = A_{c1} + A_{c2}$$

$$A_{c1} = 4 \times [0.1db - 0.045b^2] \approx 0.07A_c$$

$$A_{c2} = 4 \times [0.5d^2 - 0.08b^2 + 0.4bd] \approx 0.93A_c$$

$$A_c = 4 \times [0.5d^2 - 0.125b^2 + 0.5bd]$$
(12)

When octagonal PEC columns reached their ultimate strength, the average ratio of the axial compressive load to the yield load of steel tube is equal to one. Considering the finite element model verified in the previous section and effect of width to web thickness ratio on load bearing ability, a new confinement coefficient may be introduced for concrete confinement as per the following.

The ultimate bearing capacity (N_u) of axially-loaded octagonal PEC columns can therefore be illustrated as:

$$N_u = A_s f_y + A_s f_r + \chi A_s f_c ; (0 \leq \chi \leq 1.8)$$

$$\chi = -0.62 + \frac{1049505}{1 + 145305 \left(\frac{b_f}{t_f}\right)^{0.7}}$$
(13)

Where χ is the confinement coefficient of concrete based on the width-to-thickness ratio of flange.

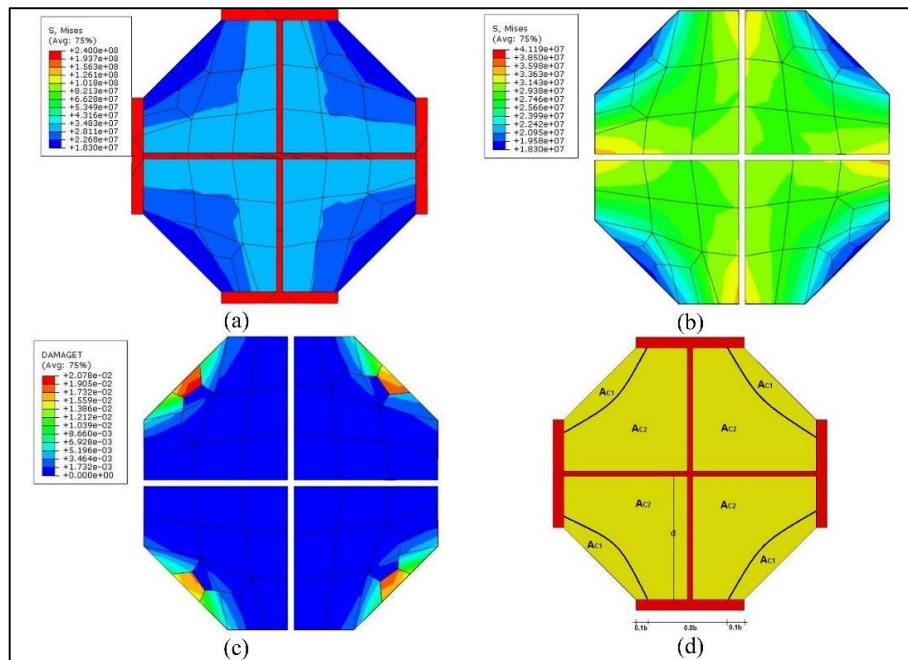


Figure 12. Division on stress region of cross section (a) stress contour of whole section (b) stress contour of concrete section (c) tensile damage in concrete (d) confined area.

2.5. Torsional Behaviour of PEC Column and Strengthening Methods for Cross-Shaped Steel Column

One of the subjects least studied in current codes regarding composite columns is behaviour of this column under torsion and methods of improving its behaviour. Since few investigations have been conducted in this field (especially about PEC column), in this section a cross-shaped steel column and an octagonal PEC column were investigated under

constant gravity load and varying monotonic torsional loading. Each column was tested in accordance with three cases illustrated in Figure 13. The second and third cases were used to find a way to enhance torsional capacity of the PEC columns. Descriptions of the tested models are given in Table 6.

Stiffening plates used at the top and bottom of the column had a length of 150 mm and a thickness which was the same as that of column flange (6 mm). Diameter and spacing of the transverse links were similar to those of the tested specimens. Results of these tests were given in the form of torsional moment-rotation diagram, formation and propagation of plastic hinge and strain along the column.

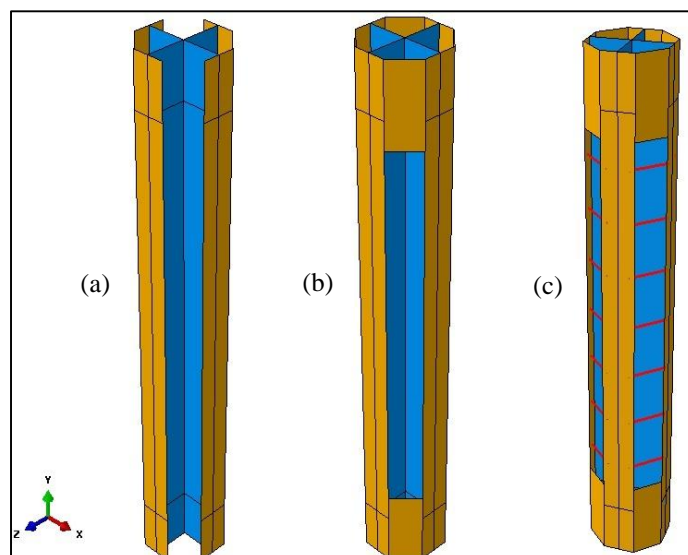


Figure 13. Three types of cross-shaped column under torsion load

Table 6. Description of specimens

Specimen	Description
BS	Bare Steel column
BS-St	Bare steel column strengthened with two stiffener at top and bottom of the column
BS-St-L	Bare steel column strengthened with two stiffener at top and bottom of the column and using of transverse links
PEC	Partially Encased Composite column
PEC-St	PEC column strengthened with Stiffeners at the top and bottom of the column
PEC-St-L	PEC column strengthened with Stiffeners at the top and bottom of the column and using of transverse links

2.5.1. Moment-Rotation Relationship

In this section, a 100 kN constant force combined with linear incremental torsional moment was applied on top of the column. A rigid beam on top of each specimen was used to apply torque. Figure 14. illustrates results of two series of the specimens. In bare steel columns, most of the torsional moment withstood by the four flanges and column webs had less effect in this regard; it was the result of less torsional stiffness of the column web due to being a thin-walled open section. BS specimen had the least rotational stiffness amongst bare steel sections but its rotational stiffness could be increased up to 91% by adding two hardening plates at the top and bottom of the column. It was the result of an increase in polar moment of inertia on the top and bottom of the section which sustained most of the torsional moment and rotation. By adding transverse links to BS-St column and creating BS-St-L column, torsional stiffness would increase only by an amount of 3%. Maximum torsional moment resisted by BS-St-L specimen was 4.9 kN – m which was almost equal to that of BS-St specimen but 20% more than that of BS specimen.

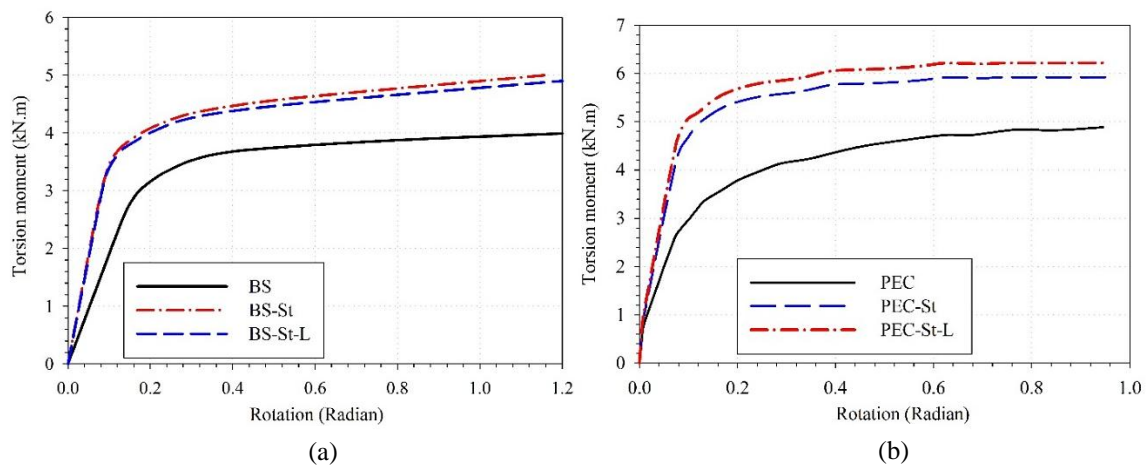


Figure 14. Torsion moment-rotation curve, (a) bare steel column, (b) PEC column

In PEC columns, it was observed that PEC-St-L specimens had the highest torsional rigidity and resistance as expected. In comparison between PEC and PEC-St-L Specimens, an increase of 50% and 27% was observed in torsional stiffness and torsional moment of resistance, respectively. Figure 14b shows that the first section of the diagram had two initial stiffness; the reduction in stiffness was resulted from tensile and shear cracking in the middle of the concrete and propagation of the damage along the concrete portion of the section. This reduction continued to the extent that most of the middle concrete portion of the column was damaged and torsional moment was solely sustained by steel section of the column.

A comparison described below is made in order to better understand the effects of concrete, hardening plates and transverse links. By adding hardening plate to the BS column, rotational stiffness was increased by an amount of 91%. By adding concrete to the BS column, this increase of rotational stiffness would be only an amount of 5%. Effects of using concrete confinement would increase torsional stiffness and resistance greatly. By using hardening plates in PEC columns, torsion stiffness is increased by 40%. Amongst these methods, use of concrete and hardening plates improved torsional properties greatly.

2.5.2. Effect of Compressive Load Ratio on Torsional Capacity

Both groups of BS and PEC columns were tested under torsional moment combined with three constant compressive force ratio (the ratio of applied compressive force to yield compressive force of the section) of 10% to 80%. Figure 15. shows variation of torsional stiffness in relation to different compressive force ratios. It was observed that variation of compressive force ratio has almost no effect on torsional behaviour of specimens in BS column until 30% load ratio. Although in PEC columns compared to BS columns we observed more effects on torsional behaviour, yet these effects were almost negligible before 30% load ratio. But, after 30% load ratio, specimens experienced a gradual decrease in rotational stiffness. This was due to occurrence of local buckling of flanges under compressive loading.

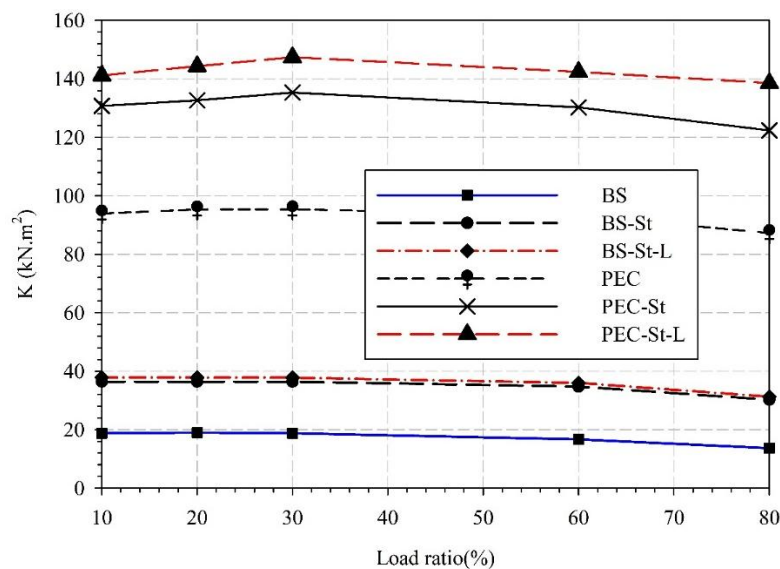


Figure 15. Load ratio- torsional stiffness of specimens

2.5.3. Failure and Fracture Mechanism

Figure 16. shows failure and fracture modes for both steel column and PEC column. In BS columns, maximum torsional rotation and torsional moment was sustained at the point of load application and at the column support, therefore these locations reached the ultimate plastic strain of steel material prior to other locations. Use of hardening plates in BS-St specimen delayed formation of plastic hinge and enhanced torsional stiffness of the specimen which led to shift of plastic region to a level beneath the hardening plates in column flanges. Moreover, it was observed that use of transverse links had little effect on changing or shifting yield mechanism. In this regard, none of the transverse links reached their yield strain which demonstrated that these links were incapable of having any effect on delaying or changing column rupture mode.

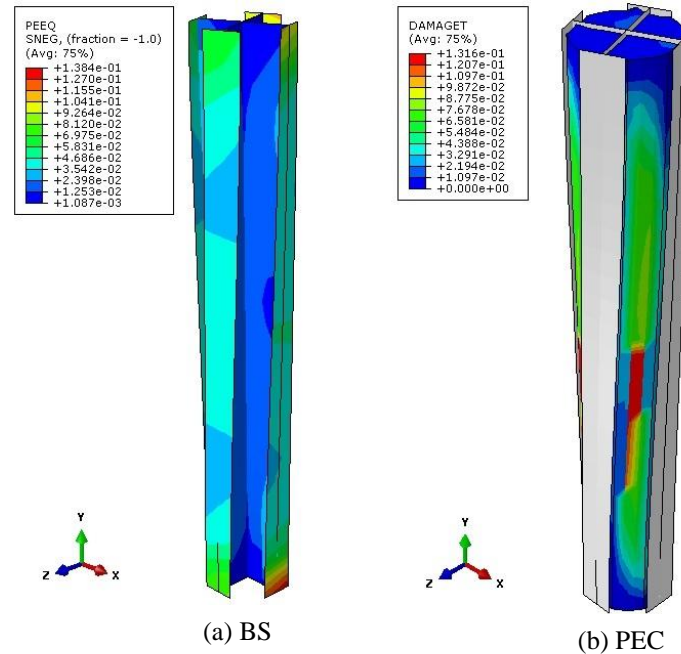


Figure 16. Failure mode of two specimens

Use of specimens confined with concrete (PEC) caused a change in force transmission and yielding of column. Due to high stiffness of concrete, first the middle portion of the concrete was damaged due to tensile and shear stresses caused by applying torsional moment, and gradually the damage was propagated toward the height of the column. After total rupture of the middle concrete portion of the column, torsional moment would be solely sustained by web and flange plates of the column. In other words, steel portion of the column would stay perfectly in linear elastic state prior to failure of most of middle concrete portion of the column.

3. Conclusion

Experimental and numerical research project were conducted to assess the behaviour of octagonal PEC cross-shaped columns made with different details. A total of three PEC columns were tested. Relevant FE analysis was also conducted. The failure modes, load-strain responses, column strength and rotation capacity were discussed. The summary of the most important study findings are given in the following.

- For all three concentric tests, the failure mode was similar: concrete crushing combined with the steel flange buckling. The local buckling occurred after or at the same time the peak load occurred between the links.
- The addition of steel rebars to the normal-strength concrete resulted in a column failure that was somewhat more ductile; therefore, the failure mode of the PEC-CL column was influenced by the failure mode of the concrete within the column. In column PEC-CLS, load capacity and corresponding displacement reached the maximum value amongst all specimens.
- The average predicted-to-test capacity ratio of the PEC columns that was made with normal-strength concrete (without reinforcement) was 1.14. For the concrete reinforcement with rebars, the average ratio was 1.02. Comparing the test results of this study with CSA S16-14 equation showed that this equation was conservative for use with PEC columns. These design calculations reduce the capacity of the steel flanges to account for their susceptibility to local buckling between the links. However, before specimens reached to their ultimate capacity, no local buckling was seen in the flange.
- A finite element model was applied to simulate suggested PEC column behaviour under compressive loading, and the results of comparing the same with that in the test results represented acceptable conformity.

- Influences of several parameters such as link spacing, diameter and flange width-to-thickness ratio on the behaviour of PEC columns were discussed. Large distance of links shall cause early local buckling, followed with lower capacity. Lack of transverse link resulted in early loss in column load-bearing capacity, which emanated from early buckling of the relevant steel beam flanges. Also, columns with bigger flange width-to-thickness ratios experienced less strength in comparison to column with bigger flange thickness. This was because of providing less confinement for concrete. Finally, a little change in welding configuration line could improve the load bearing capacity and failure mode of PEC columns.
- In this study, based on parametric studies, the flange width to thickness ratio effect on concrete confinement was offered with a factor between 0 and 1.8.
- Generally, the torsional stiffness of the columns decreased by increasing the load ratio. Especially in the load ratio greater than 50%, the torsional stiffness of decreasing rate had a faster trend. It was noted that with increasing load ratio up to 30% in the PEC columns, torsional stiffness had a relatively upward trend. This was due to the effect of compressive strength on delaying the concrete cracking. After this load ratio, the torsional stiffness experienced a downward trend.

4. References

- [1] Shafaei, Soheil, Amir Ayazi, and Farhang Farahbod. "The effect of concrete panel thickness upon composite steel plate shear walls." *Journal of Constructional Steel Research* 117 (2016): 81-90.
- [2] Rassouli, Behnoosh, Soheil Shafaei, Amir Ayazi, and Farhang Farahbod. "Experimental and numerical study on steel-concrete composite shear wall using light-weight concrete." *Journal of Constructional Steel Research* 126 (2016): 117-128.
- [3] Oyawa, Walter O., N. K. Githimba, and G. N. Mang'urio. "Structural response of composite concrete Filled plastic tubes in compression." *Steel and Composite Structures* 21, no. 3 (2016): 589-604.
- [4] Andalib, Z., Kafi, M.A., Kheyroddin, A., Bazzaz, M. " Experimental investigation of the ductility and performance of steel rings constructed from plates" *Journal of Constructional Steel Research*, 103 (2014): 77-88.
- [5] Chicoine, T., Tremblay, R., Massicotte, B., Ricles, J., Lu, L.W. "Behaviour and strength of partially encased composite columns with built up shapes" *Journal of Structural Engineering*, 128(3) (2002): 279-288.
- [6] Chicoine, T., Massicotte, B., Tremblay, R. "Finite element modelling and design of partially encased composite columns" *Steel and Composite Structures, An International Journal*, 2(3) (2002): 171-194.
- [7] Begum, M., Driver, R.G., Elwi, A.E. "Finite element modeling of partially encased composite columns using the dynamic explicit solution method" *Journal of Structural Engineering*, 133(3) (2007): 326–34.
- [8] Begum, Mahbuba, Robert G. Driver, and Alaa E. Elwi. "Behaviour of partially encased composite columns with high strength concrete." *Engineering Structures* 56 (2013): 1718-1727.
- [9] Begum, M., Driver, R., Elwi, A.E. "Parametric study on eccentrically-loaded partially encased composite columns under major axis bending" *Steel and Composite Structures, An International Journal*, 19(5) (2015): 1299-1319.
- [10] Chen, Y., Wang, T., Yang, J., Zhao, X. "Test and numerical simulation of partially encased composite columns subject to axial and cyclic horizontal loads" *International Journal of Steel Structures*, 10(4) (2010): 385–393.
- [11] Zhao, Gen Tian, and Chao Feng. "Axial Ultimate Capacity of Partially Encased Composite Columns." In *Applied Mechanics and Materials*, vol. 166, pp. 292-295. Trans Tech Publications, 2012.
- [12] Dastfan, M., Driver, R. "Large-scale test of a modular steel plate shear wall with partially encased composite columns" *Journal of Structural Engineering*, 142(2) (2016): 04015142.
- [13] Pereira, F.M., De Nardin, S., El Debs, L.H.C. "Structural behaviour of partially encased composite columns under axial loads" *Steel and Composite Structures, An International Journal*, 20(6) (2016): 1305-1322.
- [14] Song, Y.C., Wang, R.P., Li, J. " Local and post-local buckling behaviour of welded steel shapes in partially encased composite columns" *Thin-Walled Structures*, 108 (2016): 93–108.
- [15] Ebadi Jamkhaneh, M., Kafi, M.A., Kheyroddin, A. "Experimental and numerical investigations of partially encased composite columns under axial load." *Journal of Structural and Construction Engineering (JSCE)*, (in persian) (2017), DOI: 10.22065/JSCE.2017.92721.1264.
- [16] CSA, CSA S16–14, Limit States Design of Steel Structures. Canadian Standards Association, (2014) Mississauga, Ontario.
- [17] ACI Committee 318, Building Code Requirements for Structural Concrete (ACI 318-08) and Commentary (ACI 318R-08). (2008) Farmington Hills, MI: ACI.

- [18] ACI, ACI 363R-92, State-of-the-art report on high-strength concrete (reapproved in 1997). American Concrete Institute, (1997) Farmington Hills, MI.
- [19] ASTM, A370-03, Standard test methods and definitions for mechanical testing of steel products. (2003) American Society for Testing and Materials, Philadelphia, PA.
- [20] Eurocode 4. Design of composite steel and concrete structures, Part 1-1: General rules and rules for buildings.
- [21] Han, L-H. "Tests on stub columns of concrete-filled RHS sections." *Journal of Constructional Steel Research* 58, no. 3 (2002): 353-372.
- [22] Hibbitt, Karlsson and Sorensen, Inc., ABAQUS User's Manuals, Version 6.13.1. Rhode Island, USA, 2013.
- [23] Hsu, L.S., Hsu, C.T.T. "Complete stress-strain behaviour of high-strength concrete under compression" *Magazine of Concrete Research*, 46(169) (1994): 301-312.
- [24] Nayal, R., Rasheed, H.A. "Tension stiffening model for concrete beams reinforced with steel and FRP bars" *Journal of Materials in Civil Engineering*, 18(6) (2006): 831-841.